Journal of Environmental Chemical Engineering 12 (2024) 113709

Contents lists available at ScienceDirect

Journal of Environmental Chemical Engineering

journal homepage: www.elsevier.com/locate/jece

Terahertz spectroscopy-based rapid detection of exchangeable heavy metal pollution in soil using *Scenedesmus obliquus*

Yuxin Zhou [a], Di Zhu [a], Yan Peng [a,b], Yiming Zhu [a,b], Yongni Shao [a,b,*]

[a] *Terahertz Technology Innovation Research Institute, Terahertz Spectrum and Imaging Technology Cooperative Innovation Center, Shanghai Key Lab of Modern Optical System, University of Shanghai for Science and Technology, Shanghai 200093, China*
[b] *Shanghai Institute of Intelligent Science and Technology, Tongji University, Shanghai 200092, China*

ARTICLE INFO

Keywords:
Terahertz spectroscopy
Scenedesmus obliquus
Soil
Exchangeable heavy metal
Physical adsorption

ABSTRACT

This study introduces a novel approach for the rapid detection of exchangeable heavy metal pollution in soil, utilizing *Scenedesmus obliquus* as a bioadsorbent. Terahertz spectroscopy was used to analyze the cell wall proteins and functional groups of *S. obliquus* following physical adsorption. This analysis enabled the deduction of the types and concentrations of exchangeable heavy metal ions in soil. We established a prediction model for heavy metal concentrations using partial least squares (PLS) regression, achieving optimal detection times: 10 min for Pb^{2+}, 20 min for Ni^{2+}, and 30 min for Co^{2+}. Validation with real surface soil samples demonstrated excellent accuracy rates: 97.8 % for Pb^{2+}, 91.8 % for Ni^{2+}, and 90 % for Co^{2+}. Notably, our method reduces the detection time to 0.5 hours, requires only 5 ml of sample volume, and enhances detection accuracy to 0.1 μg/L.

1. Introduction

Due to rapid urbanization and extensive industrial activities, soil contamination is escalating, resulting in increased levels of various heavy metals, including lead (Pb), nickel (Ni), and cobalt (Co) [1]. These heavy metals pose serious health risks due to their toxicity and potential bioaccumulation in the food chain. For example, prolonged exposure to nickel can induce cutaneous inflammation in humans, leading to festering of the skin [2]. Lead is known to accumulate in humans, disrupting the regular maturation of erythrocytes, which in turn may contribute to the onset of leukemia[3]. Excessive inhalation of cobalt dust can cause "cemented carbide disease", which can cause dyspnea, allergic asthma, and pulmonary edema [4,5]. The forms of heavy metals in soil include exchangeable heavy metals, carbonate-bound heavy metals, iron-manganese oxide-bound heavy metals, organic-bound heavy metals, and residual heavy metals [6]. Among these forms, exchangeable heavy metals are of particular concern due to their susceptibility to environmental fluctuations, mobility, and propensity for transformation. Their capacity to migrate via water flow to groundwater and surface water poses a significant risk of water pollution [7]. Thus, this study focuses on the issue of exchangeable heavy metal ions in soil, aiming to better understand their behavior and potential impacts on environmental quality.

At present, atomic absorption spectroscopy (AAS), inductively coupled mass spectrometry (ICP-MS), atomic emission spectroscopy (AES), and X-ray fluorescence (XRF) are the mainstream approaches for the detection of heavy metals in soil [8–11]. Traditional methods are limited by the need for extensive chemical pretreatment, which is both time-consuming and cumbersome, and by the requirement for sample digestion to achieve a homogeneous aqueous solution. Furthermore, these methods typically analyze one element at a time and have high detection limits, making them unsuitable for trace detection [12,13]. Biological monitoring entails the assessment of soil pollution by analyzing alterations in specific organisms inhabiting the contaminated soil [14]. Microalgae, with their low cultivation costs and easy availability, have a high adsorption capacity due to their large cell surface area, providing numerous adsorption sites for efficient heavy metal pollutant removal. The surface of microalgae cells contains abundant negatively charged groups that can form complexes with heavy metal ions, effectively removing heavy metal pollutants [15]. Additionally, microalgae exhibit adaptability and stress resistance to various extreme environmental conditions, such as high temperature, salinity, and pH levels [16]. This enables microalgae to grow and adsorb heavy metals under different environmental conditions, demonstrating high

* Corresponding author at: Terahertz Technology Innovation Research Institute, Terahertz Spectrum and Imaging Technology Cooperative Innovation Center, Shanghai Key Lab of Modern Optical System, University of Shanghai for Science and Technology, Shanghai 200093, China.
E-mail address: ynshao@usst.edu.cn (Y. Shao).

https://doi.org/10.1016/j.jece.2024.113709
Received 24 November 2023; Received in revised form 15 July 2024; Accepted 29 July 2024
Available online 30 July 2024

application prospects in pollution detection.

In the context of heavy metal absorption by microalgae, two distinct forms of uptake are observed [5,17]. The first mechanism involves adsorption on the cell surface, commonly referred to as physical adsorption. This process relies on the physical interactions between microalgae and heavy metal ions, involving complex formation, chelation, ion exchange, redox reactions, and microprecipitation mechanisms. Notably, physical adsorption occurs independently of cellular energy metabolism, as the binding of metal ions to microalgae does not require energy expenditure [18]. The second form of absorption, known as biosorption, occurs within the intracellular environment of microalgae. During the biosorption process, the uptake of metal ions primarily relies on diffusion for their transportation into the cellular environment. This phenomenon is frequently associated with energy consumption since cells must engage in specific energy-dependent mechanisms to facilitate the intracellular movement of metal ions [19]. Currently, we have successfully developed a new method for real-time detection of heavy metal types and concentrations in water using the biological adsorption mechanism of microalgae and terahertz spectroscopy [20]. This holds considerable significance within the realm of soil heavy metal detection.

However, when detecting heavy metal pollution in soil, the biosorption method of microalgae is not applicable, due to the complexity of the soil and the relatively long time required for biosorption can affect the biosorption ability of microalgae. Soil is a complex medium composed of organic matter, clay, minerals, and other components, which might interact with the cell wall or membrane of microalgae, thereby affecting the bioadsorption efficiency and accuracy of heavy metals adsorption by microalgae [21,22]. This interaction limits the application of microalgae in detecting heavy metal pollution in soil. In contrast, the use of shorter-time microalgae physical adsorption methods can more effectively address the challenge of detecting heavy metal pollution in soil. The physical adsorption method of microalgae utilizes the electrostatic interaction between negatively charged groups on the surface of microalgae cells and heavy metal ions for adsorption. The adsorption rate of this physical adsorption is faster than that of biological adsorption, usually taking only a few minutes to a few hours, allowing microalgae to more efficiently adsorb heavy metal pollutants in complex soil samples [23]. Thus, we leverage microalgae's physical adsorption to sequester exchangeable heavy metal ions. This method does not require the use of hazardous chemicals for complex pretreatment of soil samples, which helps simplify and accelerate sample pretreatment.

The primary factors impacting the physical adsorption of heavy metals by microalgae include the functional groups and glycoproteins present in the cell wall structure [24]. Conventional methodologies employed for the detection of functional groups within cell walls often involve the use of techniques such as immunolabeling and high-performance liquid chromatography. However, these methods involve intricate extraction procedures [25]. In addition to these approaches, spectral techniques have been utilized for detecting functional groups in cell walls, owing to their fast and non-destructive testing characteristics. These techniques primarily encompass infrared spectroscopy and Raman spectroscopy [26]. Infrared and Raman spectroscopy are highly sensitive and non-destructive optical detection techniques that provide valuable molecular and lattice vibration information [27]. It's worth noting that infrared spectroscopy, due to the intense O-H stretching vibration, may have limitations in detecting liquid components [28]. Conversely, Raman spectroscopy, with its weak water signal, offers significant advantages in detecting samples rich in water content [29]. However, the fluorescence background from the samples, along with the presence of ubiquitous random noise interference, can lead to baseline drift. Such drift can affect the accuracy of Raman detection [30,31].

Terahertz (THz) technology has experienced a significant surge in research and applications across various disciplines, owing to rapid progress in photonics technology and materials science [32,33]. Terahertz waves, occupying the frequency range of 0.1–10 THz, reside in the intermediate region between far-infrared and microwaves [13]. The cell wall functional groups -OH and -COOH, which need to be detected, are typical polar groups that form hydrogen bonds in water [34]. The vibration absorption frequency of intramolecular chemical bonds mainly lies in the infrared band, while weak intermolecular interactions, such as hydrogen bonds, van der Waals forces, and rotation and vibration transition of dipoles, as well as low-frequency vibration absorption of the crystal lattice, are mainly in terahertz band [33,35]. Additionally, the wavelength of the terahertz spectrum is longer than that of the infrared spectrum, making it less susceptible to scattering [36]. The terahertz region corresponds to the intermolecular vibration mode and lattice vibration. Since most organic molecules possess specific "fingerprint" spectra, different substances can be qualitatively and quantitatively analyzed based on their terahertz characteristic peaks [37].

This research categorizes heavy metals into two distinct groups based on their toxicity: highly toxic and generally toxic [38]. Lead ions (Pb^{2+}) were chosen as representatives of highly toxic heavy metal ions, while nickel ions (Ni^{2+}) and cobalt ions (Co^{2+}) were selected to exemplify generally toxic heavy metal ions. *S. obliquus* was selected as a representative microalgae carrier, and it was exposed to various durations and concentrations of metal ions. Terahertz spectroscopy was employed to analyze alterations in the surface material composition and functional groups of *S. obliquus* cells over time. A correlation model was established to link changes in material composition and functional groups (including proteins, -OH groups, polysaccharides, and COO-) to the concentration of heavy metal ions. Subsequently, the efficacy of the approach was validated by analyzing soil samples collected from industrial sites with atomic absorption spectroscopy. Fig. 1 illustrates the schematic representation of our experimental procedure. The obtained results indicate the superiority of terahertz technology over traditional detection methods. Our discoveries offer invaluable understanding for the assessment of heavy metal types and concentrations in soil, presenting a promising new methodology and technical support for environmental analysis.

2. Material and methods

2.1. Biological and chemical materials

The microalgae utilized in this experimentation is *S. obliquus* (strain number: 276), procured from Freshwater Algae Culture Collection at the Institute of Hydrobiology (FACHB). The chemical reagents utilized included nickel nitrate hexahydrate (98 % purity, analytical reagent grade, molecular weight 290.81), lead nitrate (99 % purity, analytical reagent grade, molecular weight 331.21), and cobaltous nitrate (99 % purity, analytical reagent grade, molecular weight 291.05), all of which were purchased from the Aladdin Reagent Network.

2.2. Microalgae cultivation and sample preparation

2.2.1. Sources and cultivation of S. obliquus

Before the commencement of the experiment, a microscopic examination of *S. obliquus* is conducted to ascertain the absence of bacteria, fungi, or any other microorganisms that could potentially contaminate the culture. Throughout the cultivation process of *S. obliquus*, stringent measures are taken to ensure sterility. All equipment, media, and glassware used in the cultivation of *S. obliquus* are thoroughly sterilized using high-pressure techniques, aimed at eradicating any potential pollutants. The BG11 medium is used to facilitate the optimal growth of *S. obliquus*. This culture medium is meticulously formulated to selectively promote the growth of *S. obliquus* while inhibiting the proliferation of pollutants. Preparing the BG11 culture medium entails adjusting it to a suitable concentration before introducing it into a conical flask. Subsequently, the conical flask is subjected to high-pressure sterilization

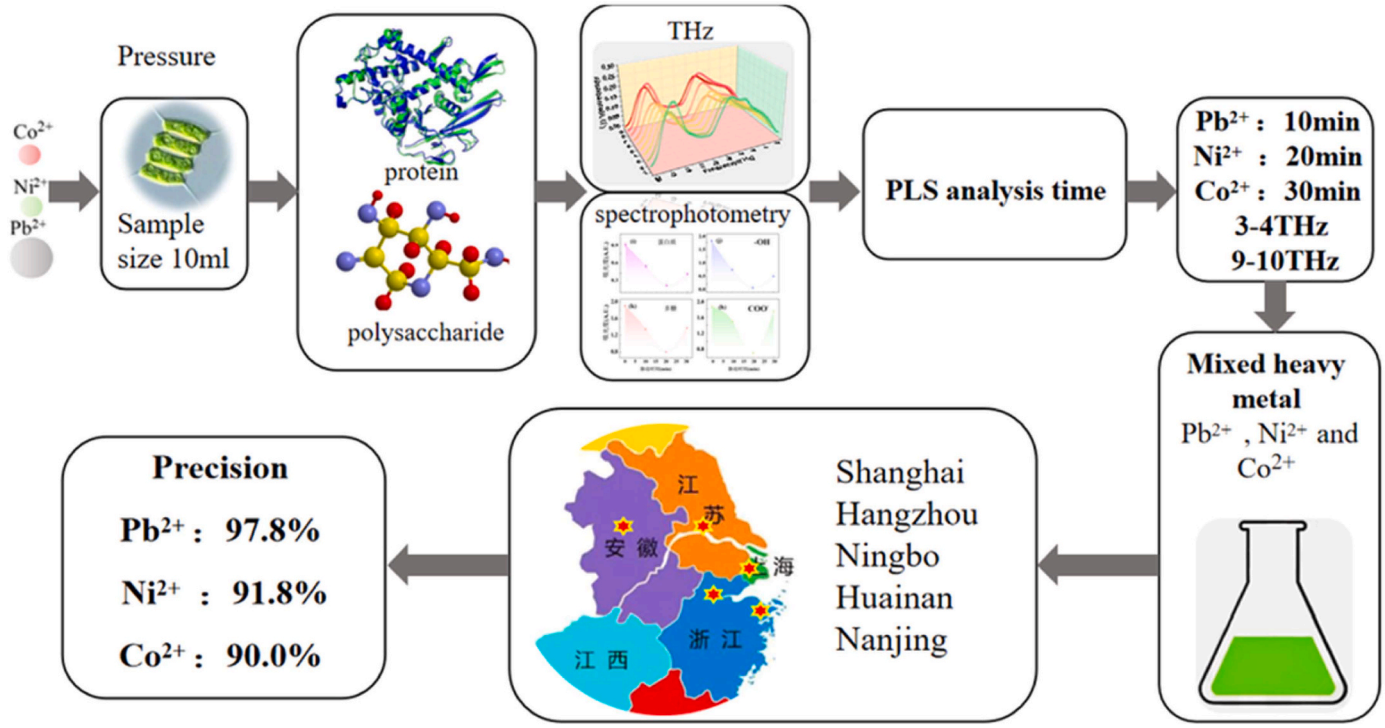

Fig. 1. The flow chart of the study.

at 120°C. Upon cooling, an appropriate quantity of *S. obliquus* is added for cultivation. To reduce the risk of dust pollution, the mouth of the conical flask is sealed with non-woven fabric secured by rubber bands. Placed in an ultraclean laboratory, the cultivation lasts about 2 months. The cultivation temperature is 20°C, the light intensity is 3000 lux, and the light-dark cycle is 12 hours:12 hours. During the cultivation period, the growth morphology of *S. obliquus* was regularly observed with a cell counting plate and a microscope, and the cell density was estimated to ensure stability throughout the experiment.

2.2.2. Physical adsorption and sample preparation

Allow the well-grown and stable *S. obliquus* to settle at the bottom of the conical flask, then discard the upper layer of clean water. The remaining *S. obliquus* suspension was centrifuged at 6500 rpm for 5 minutes. After centrifugation, the upper clear liquid was removed, and sterile distilled water was added, repeating the washing process three times to collect impurity-free *S. obliquus*. Prepare for physical adsorption by loading 10 ml of *S. obliquus* into test tubes. According to the experimental plan, equal amounts of *S. obliquus* and an aqueous solution containing different concentrations of heavy metal ions were mixed and shaken evenly. Samples were collected using disposable gel droppers at 10, 20, and 30 minutes, respectively. Centrifuge each sample, washing it three times with sterile distilled water through repeated cycles of addition and centrifugation. Place the cleaned *S. obliquus* mud into a polyethylene mold and dry at a low temperature in an oven. Put the dried sample into a grinder and grind it at a frequency of 70 Hz for 3 minutes. Mix *S. obliquus* powder with Cyclic Olefin Copolymer (COC) powder (5 mg *S. obliquus*: 50 mg COC), place it into a mold, and press with 4 tons of pressure for 2 minutes to form a 1 mm thick film. Subsequently, the compressed sample is analyzed using terahertz spectroscopy.

2.3. Dissolution rate of heavy metals in soil

The dissolution rate of heavy metals in soil is influenced by several factors, including soil pH, organic matter content, chemical speciation of heavy metals, soil moisture content, and ion strength, among others. Experimental measurements can determine the dissolution rate of heavy metals in soil under specific conditions. Generally, the dissolution rate of heavy metals in soil can be quantified using the following formula:

$$[S] = CiVp/ms$$

Here, [S] represents the dissolution rate of heavy metals in soil (mg/kg); Ci is the concentration of Pb, Ni, and Co in aqueous solution (mg/L); Vp is the volume of the extraction solution for water-soluble heavy metals in soil (liters); ms is the mass of the soil sample (kilograms).

2.4. THz spectral measurement

We employed a Fourier-transform infrared (FTIR) spectrometer, model Vertex 80 v, manufactured by BRUKER in Germany. The spectrometer's light source was a water-cooled mercury lamp, ensuring stable and continuous infrared light emission. To mitigate moisture interference, nitrogen was continuously purged through the instrument during data collection. Before each test, a blank carrier was used for background scanning and noise elimination. Data acquisition was performed using the spectroscopic software OPUS, developed by BRUKER, Germany.

2.5. Partial least squares

Partial Least Squares (PLS) is a statistical technique used in multiple linear regression. The primary objective of PLS is to establish a robust relationship between the data and the model by leveraging the correlation coefficient between predicted and actual values. By incorporating multiple regression analysis, PLS enhances the model's predictive accuracy, making it well-suited for handling complex datasets.

In the evaluation phase, two key performance metrics are commonly used to assess the PLS model's reliability and effectiveness. The first metric is the coefficient of determination (R^2), which measures the proportion of the variance in the dependent variable explained by the independent variables. A higher R^2 value indicates a better fit to the data. The second metric, the root mean square error (RMSE), calculates the square root of the average squared differences between predicted

and actual values. A lower RMSE value indicates a more accurate and precise model.

3. Research and results

3.1. S. obliquus Spectra to Pb^{2+} solution stress

We chose Pb^{2+} as the more toxic heavy metal ion. In this research, we conducted terahertz spectral acquisition and analyzed spectral peaks in *S. obliquus* samples exposed to various concentrations of Pb^{2+} solutions. The Pb^{2+} concentrations in the solutions were 500 μg/L, 100 μg/L, 50 μg/L, 10 μg/L, 5 μg/L, 1 μg/L, 0.5 μg/L, and 0.1 μg/L, and we obtained the THz spectra for the experimental and control groups at different adsorption time points (10 min, 20 min, 30 min). Fig. 3 shows the terahertz spectra of *S. obliquus* at eight different Pb^{2+} concentrations. All spectra exhibit a prominent envelope around 3.35 THz, which corresponds to two raised peaks at 6.76 THz and 9.18 THz, along with distinct characteristic peaks at 17.28 THz. These four characteristic peaks can be attributed to the presence of proteins, -OH groups, polysaccharides, and COO- functional groups in *S. obliquus* [39–42], consistent with the terahertz spectral peaks of *S. obliquus* without heavy metal stress, as shown in Fig. 2.

3.1.1. Study on changes in S. obliquus composition under Pb^{2+} solution stress based on terahertz spectroscopy

Three distinct levels of Pb^{2+} were chosen: a higher concentration of 500 μg/L, a medium concentration of 5 μg/L, and a lower concentration of 0.1 μg/L. By extracting four characteristic peaks, we examined the absorbance variations of these peaks over time (10 min, 20 min, and 30 min), as illustrated in Fig. 4.

According to the spectral analysis, in Pb^{2+} solutions with higher concentrations, different biomolecules, including proteins, -OH groups, polysaccharides, and COO- ions, demonstrated a pronounced decrease in absorbance within the initial 20 min. Subsequently, during the 20–30-minute period, their absorbance values exhibited a subsequent increase. At the 10-minute interval, proteins and polysaccharides reached their lowest absorbance values, which increased with the increase in Pb^{2+} concentration. On the other hand, -OH groups exhibited their lowest absorbance at high concentrations and decreased as the concentration decreased, while COO- ions reached their lowest absorbance at medium concentrations.

Transitioning to the medium concentration Pb^{2+} solution, proteins, -OH groups, polysaccharides, and COO- ions exhibited a decrease until 20 min, followed by an increase until 30 min. At the 20 min mark, proteins, -OH groups, polysaccharides, and COO- ions reached their lowest absorbance values, which increased with decreasing Pb^{2+} concentration, as depicted in Fig. 4(e), (f), (g), and (h).

In the lower Pb^{2+} concentration solution, proteins and polysaccharides exhibited a gradual decrease until 10 min, followed by an increase between 10 and 20 min, and then a subsequent decrease

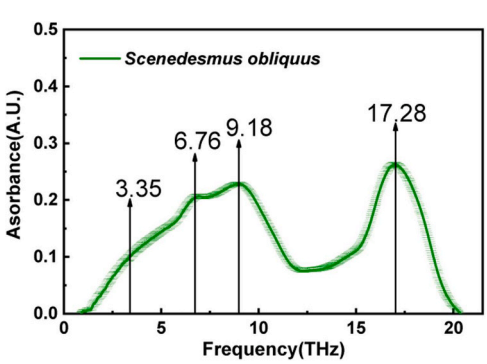

Fig. 2. THz spectral of *S. obliquus* without heavy metal stress.

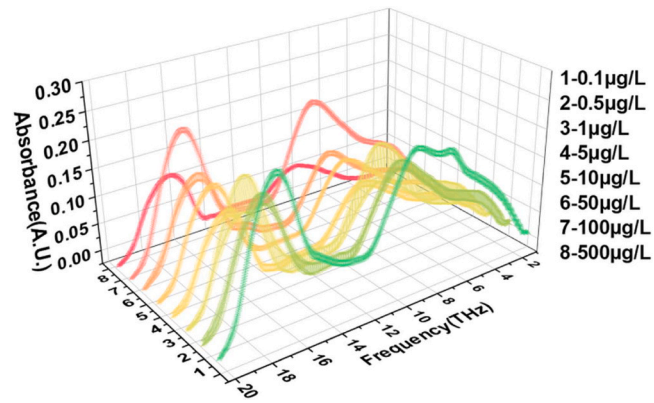

Fig. 3. THz spectral of *S. obliquus* stressed by Pb^{2+}.

between 20 and 30 min. At the 30-minute mark, proteins, -OH groups, and COO- ions reached their lowest absorbance values at low concentrations, and the peak value increased with increasing concentration. On the other hand, polysaccharides showed their lowest absorbance at high concentrations and increased with concentration, as illustrated in Fig. 4 (i), (j), (k), and (l). Notably, -OH groups decreased until 20 min and then increased, whereas COO- ions decreased until 20 min. The results indicate that the absorbance amplitude of polysaccharides exhibited the most significant changes across all concentration levels and time intervals.

3.1.2. Establish a prediction model of Pb^{2+} concentration based on PLS at various time intervals

We investigated the potential of using *S. obliquus* samples to predict Pb^{2+} concentrations using a prediction model based on PLS analysis. Absorbance measurements of the samples were conducted at various time intervals across a spectral range spanning from 75 cm^{-1} to 680 cm^{-1}. A PLS prediction model was constructed using these absorbance values. To create the PLS model matrix, we maintained a ratio of 2:1 between the calibration set and the prediction set. The eight concentrations of Pb^{2+} (500 μg/L, 100 μg/L, 50 μg/L, 10 μg/L, 5 μg/L, 1 μg/L, 0.5 μg/L, and 0.1 μg/L) were assigned corresponding identifiers ("8", "7", "6", "5", "4", "3", "2", "1"). To assess the accuracy of the PLS prediction model, we compared the correlation coefficients and RMSE of the calibration set and the prediction set.

The results obtained from the PLS modeling are presented in Table 1. Our analysis reveals that the 10-minute time point yields the optimal modeling performance, exhibiting the highest accuracy. Due to the high concentration of Pb^{2+}, the glycoprotein on the cell wall can adsorb lead ions in water quickly, showing the shortest stress time in the best adsorption time. Moreover, the detection accuracy of Pb^{2+} has been improved from 1 μg/L to 0.1 μg/L.

3.2. S. obliquus spectra to Ni^{2+} solution stress

The above describes the research on Pb^{2+}, which exhibits strong toxicity. Next, we will conduct the same analysis on Ni^{2+}, which has relatively weak toxicity. The concentrations of Ni^{2+} are as follows: 200 μg/L, 100 μg/L, 20 μg/L, 10 μg/L, 2 μg/L, 1 μg/L, 0.2 μg/L, and 0.1 μg/L. The results are shown in Fig. 5, where the position of the characteristic peak is consistent with that in Fig. 3. However, due to the weaker toxicity of Ni^{2+} compared to Pb^{2+}, the peak height is relatively low.

3.2.1. Study on changes in S. obliquus composition under Ni^{2+} solution stress based on terahertz spectroscopy

We selected three different Ni^{2+} concentrations: 200 μg/L as the higher concentration, 2 μg/L as the medium concentration, and 0.1 μg/L

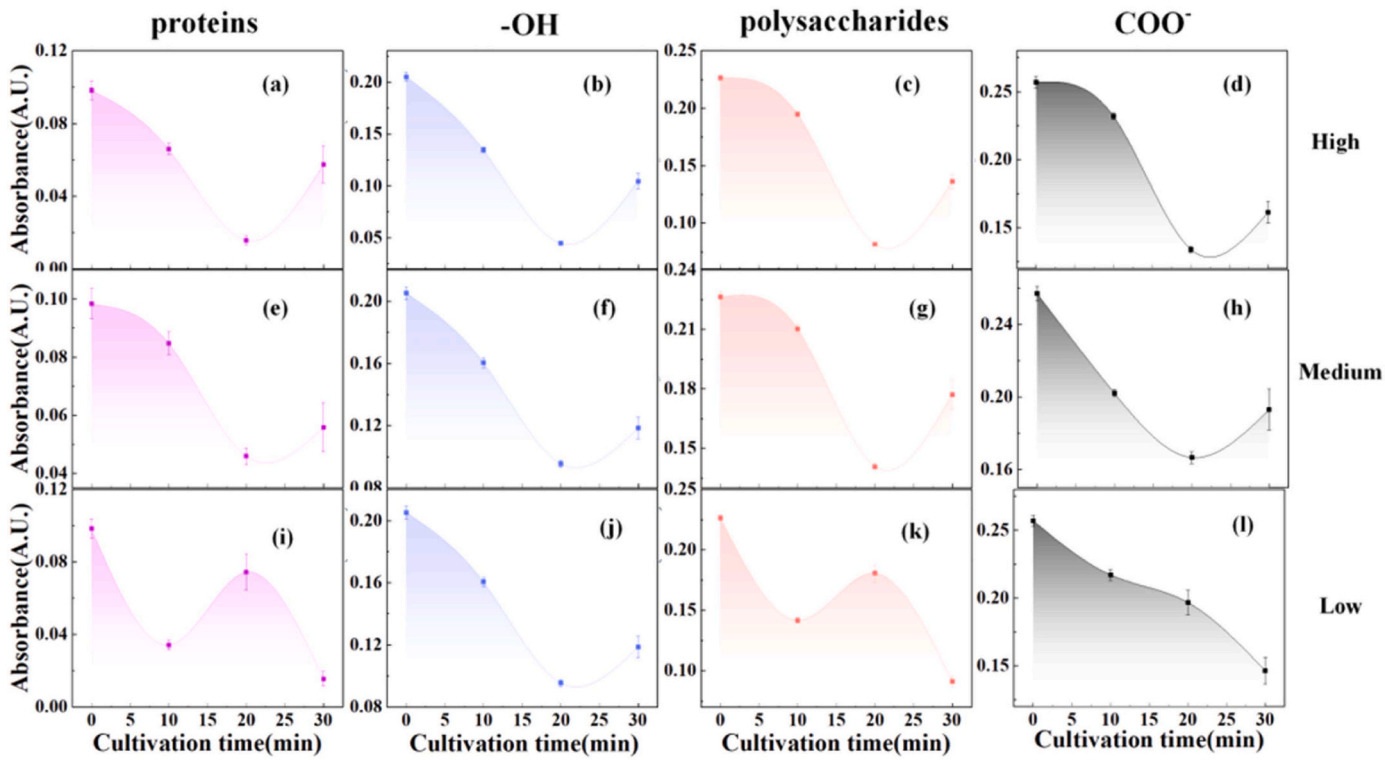

Fig. 4. Spectra of *S. obliquus* proteins, - OH, polysaccharides, and COO - under Pb^{2+} stress. High concentrations (500 μg/L) were represented by spectra (a), (b), (c), and (d); medium concentrations (5 μg/L) by spectra (e), (f), (g), and (h); and low concentrations (0.1 μg/L) by spectra (i), (j), (k), and (l).

Table 1
PLS model parameters under Pb^{2+}stress.

Discrimination model	Calibration		Prediction	
	R_c^2	RMSEC	R_p^2	RMSEP
10 min	0.894	0.745	0.867	0.834
20 min	0.879	0.894	0.899	0.817
30 min	0.882	0.885	0.881	0.887

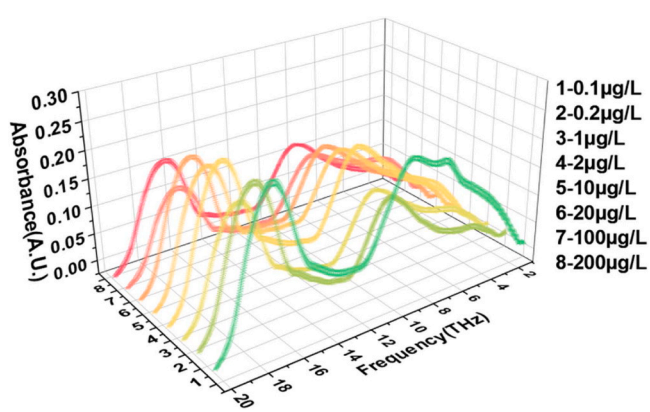

Fig. 5. THz spectral of *S. obliquus* stressed by Ni^{2+}.

as the lower concentration. Four characteristic peaks were extracted, and their absorbance variations over time were studied, as depicted in Fig. 6.

For the higher Ni^{2+} concentration, the absorbance of these peaks showed an initial increase during the first 10–30 min. Notably, the COO- peak reached its lowest point within 20 min, followed by an increase from 20 to 30 min, as evident from Fig. 6(a), (b), (c), and (d). In the medium Ni^{2+} concentration solution, the absorbance of proteins, -OH, polysaccharides, and COO- decreased in the initial 10 min and then gradually increased during 10–30 min, as indicated in Fig. 6(e), (f), (g), and (h). In the lower Ni^{2+} concentration solution, as depicted in Fig. 6 (i), (j), (k), and (l), proteins, -OH, and polysaccharides exhibited a slow decreasing trend until 20 min, followed by an increase during 20–30 min. Similarly, the COO- peak decreased until 20 min and then increased from 20 to 30 min. Within this set of substances, polysaccharides exhibited the most pronounced variations in absorbance across all concentration levels.

3.2.2. *Establish a prediction model of Ni^{2+} concentration based on PLS at various time intervals*

The same analytical method used for Pb^{2+} was employed to study Ni^{2+} samples. The calibration set for Ni^{2+}analysis includes different concentration ranges: 200 μg/L, 100 μg/L, 20 μg/L, 10 μg/L, 2 μg/L, 1 μg/L, 0.2 μg/L, and 0.1 μg/L, labeled as "8" to "1" respectively. The results, as presented in Table 2, the Ni^{2+} model demonstrated superior performance at 20 min, consistent with the understanding that Pb^{2+} toxicity exceeds that of Ni^{2+}.

3.3. *S. obliquus spectra to Co^{2+} solution stress*

The concentrations of Co^{2+} in the solutions were set at 1 μg/L, 5 μg/L, 10 μg/L, 50 μg/L, 100 μg/L, 500 μg/L, 1000 μg/L, and 5000 μg/L. Fig. 7 illustrates the spectra of *S. obliquus* exposed to eight distinct concentrations of Co^{2+}.

3.3.1. *Study on changes in S. obliquus Composition under Co^{2+} Solution Stress based on Terahertz Spectroscopy*

As illustrated in Fig. 8, three different Co^{2+} concentrations were chosen: a higher concentration of 5000 μg/L, a medium concentration of 50 μg/L, and a lower concentration of 1 μg/L.

In the presence of higher Co^{2+} concentration, proteins, -OH groups, polysaccharides, and COO- ions exhibited the lowest absorbance within

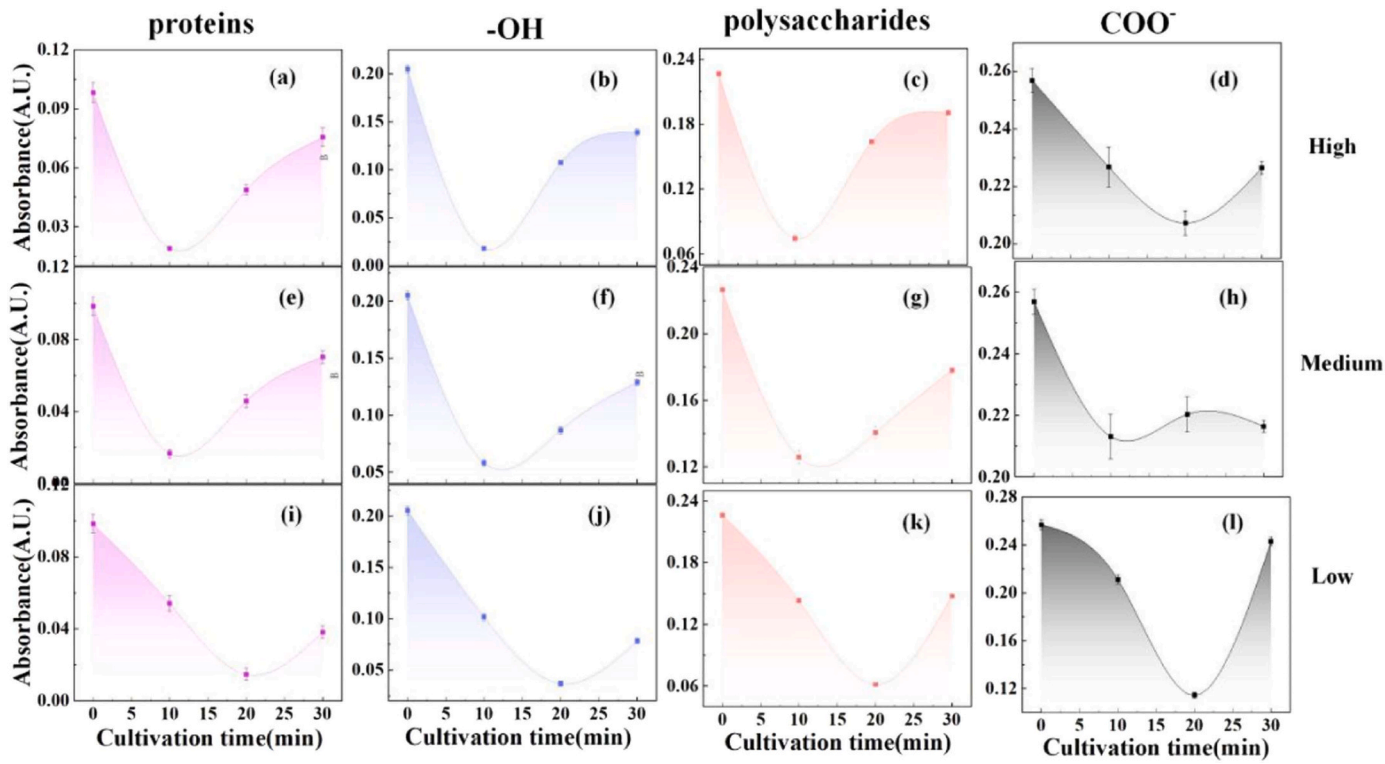

Fig. 6. Spectra of *S. obliquus* proteins, - OH, polysaccharides, and COO - under Ni^{2+} stress. High concentrations (200 μg/L) were represented by spectra (a), (b), (c), and (d); medium concentrations (2 μg/L) by spectra (e), (f), (g), and (h); and low concentrations (0.1 μg/L) by spectra (i), (j), (k), and (l).

Table 2
PLS model parameters under Ni^{2+}stress.

Discrimination model	Calibration		Prediction	
	R_c^2	RMSEC	R_p^2	RMSEP
10 min	0.857	0.974	0.835	1.04
20 min	0.921	0.724	0.887	0.865
30 min	0.834	1.05	0.815	1.09

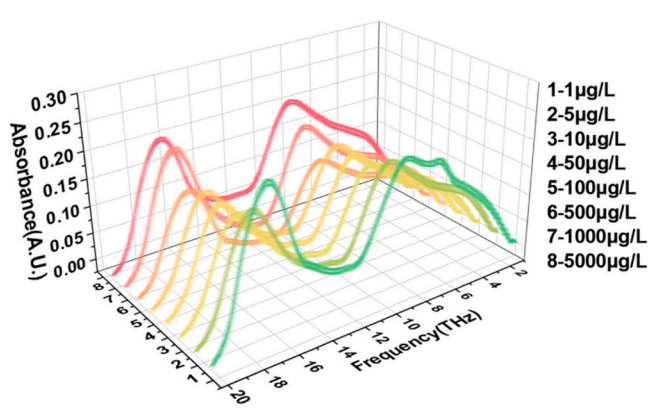

Fig. 7. THz spectral of *S. obliquus* stressed by Co^{2+}.

the first 10 min, followed by an increase from 10 to 30 min, as depicted in Fig. 8(a), (b), (c), and (d). Similarly, in the medium Co^{2+} concentration solution, proteins, -OH groups, polysaccharides, and COO- ions experienced a decline in absorbance within the initial 10 min, followed by an increase from 10 to 30 min, as shown in Fig. 8(e), (f), (g), and (h). As for the lower Co^{2+} concentration, Fig. 8(i), (j), (k), and (l) illustrate a rapid decrease in absorbance of proteins, -OH groups, polysaccharides, and COO- ions until 10 min, with subsequent increases observed at 10–20 min. Polysaccharides, akin to Pb^{2+} and Ni^{2+}, demonstrate the most notable alterations in absorbance.

3.3.2. *Establish a prediction model of Co^{2+} concentration based on PLS at various time intervals*

Use the same experimental method as that used for Pb^{2+} and Ni^{2+} to analyze Co^{2+} samples. The calibration set for Co^{2+}analysis includes a series of concentrations: 5000 μg/L, 1000 μg/L, 500 μg/L, 100 μg/L, 50 μg/L, 10 μg/L, 5 μg/L, and 1 μg/L, denoted as "8" to "1" respectively.

The obtained results are summarized in Table 3. The results indicate that PLS modeling demonstrates the most effective performance at the 30-minute mark. The reduced toxicity of Co^{2+} in comparison to Pb^{2+} and Ni^{2+} leads to a lesser impact on cellular material composition and functional groups during shorter adsorption periods than that observed with Pb^{2+} and Ni^{2+}. This phenomenon can be attributed to the milder interaction of Co^{2+} with the cellular components, thereby resulting in less pronounced changes in composition and functional groups during the initial stages of adsorption. These findings align with the understanding that Pb^{2+} and Ni^{2+} are more toxic than Co^{2+}. In conclusion, the developed PLS prediction model based on *S. obliquus* absorbance values proves effective in estimating Co^{2+} concentrations. The model's performance is superior at the 30-minute interval and offers enhanced precision for detecting Co^{2+} at lower concentrations. These results hold promising implications for environmental monitoring and toxicological assessments.

3.4. *Establish a PLS-based prediction model for Pb^{2+}, Ni^{2+} and Co^{2+} mixed solutions with different concentrations*

Based on observed spectral changes, it was determined that proteins and polysaccharides exhibited the most significant influence and played a dominant role in the response of *S. obliquus* to stress induced by Pb^{2+}, Ni^{2+}, and Co^{2+}. The results obtained from PLS modeling indicated

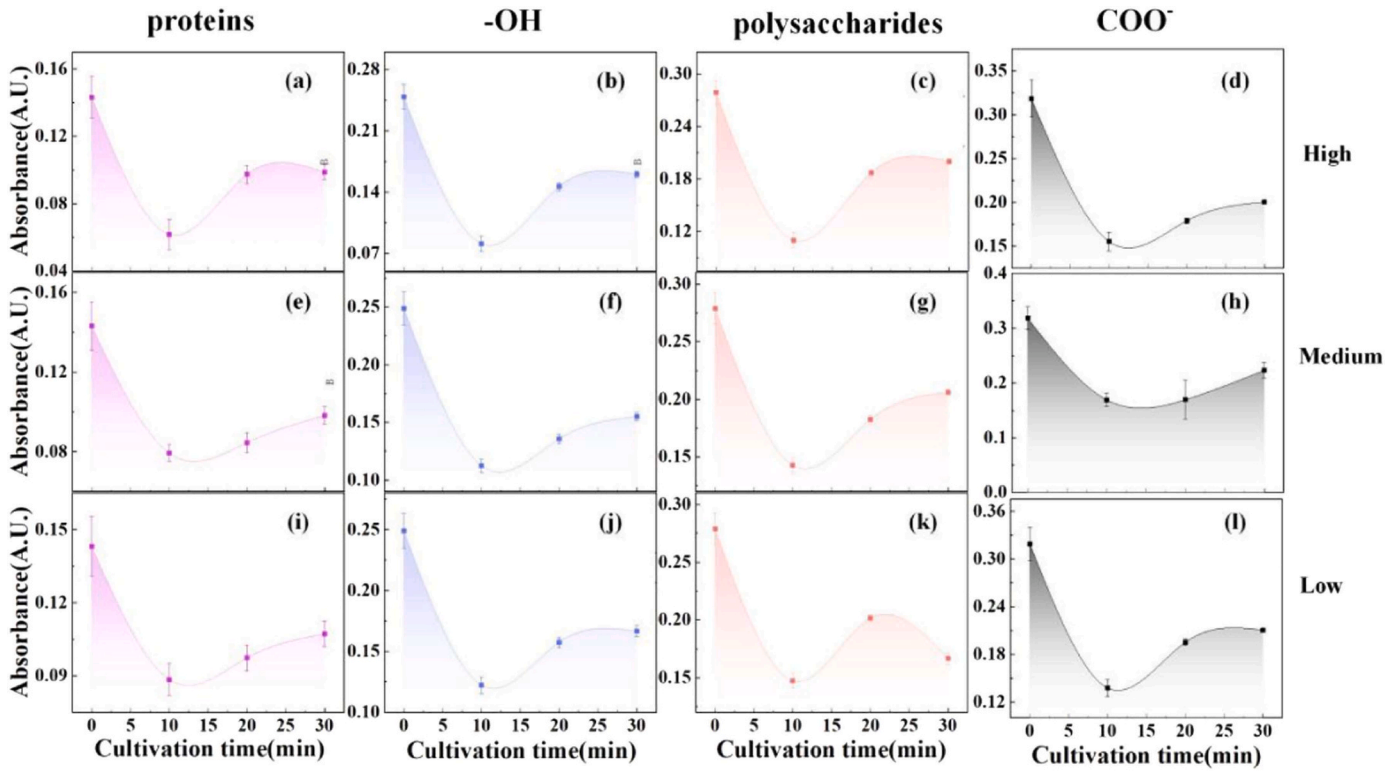

Fig. 8. Spectra of *S. obliquus* proteins, - OH, polysaccharides, and COO - under Co^{2+} stress. High concentrations (5000 μg/L) were represented by spectra (a), (b), (c), and (d); medium concentrations (50 μg/L) by spectra (e), (f), (g), and (h); and low concentrations (1 μg/L) by spectra (i), (j), (k), and (l).

Table 3
PLS model parameters under Co^{2+}stress.

Discrimination model	Calibration		Prediction	
	R_c^2	RMSEC	R_p^2	RMSEP
10 min	0.762	1.257	0.795	1.167
20 min	0.856	0.978	0.863	0.955
30 min	0.897	0.828	0.855	0.981

distinct optimal time points for each stress experiment: 10 min for Pb^{2+} stress, 20 min for Ni^{2+} stress, and 30 min for Co^{2+} stress. In light of these findings, we designed a mixed solution containing different concentrations of Pb^{2+}, Ni^{2+}, and Co^{2+} to impose stress on *S. obliquus*, utilizing the concentrations within the range employed during the individual ion modeling as outlined in Table 4. Considering that proteins and polysaccharides are the most important factors in the spectrum. Therefore, in the mixed solution stress experiment, a band model containing only proteins and polysaccharides was used (selecting 3.5–5 THz and 8–10 THz). Each sample during the modeling process was labeled as "1" to "12".

Table 4
Mixing ratio of Pb^{2+}, $Ni^{2+}$and Co^{2+}.

Samples	Pb^{2+}(μg/L)	Ni^{2+}(μg/L)	Co^{2+}(μg/L)
1	10	20	0
2	1	20	0
3	10	2	0
4	1	2	0
5	0	20	50
6	0	2	50
7	0	20	5
8	0	2	5
9	10	0	50
10	1	0	50
11	10	0	5
12	1	0	5

Based on the findings from Table 5, the calibration determination coefficients (R_c^2) were computed for three distinct time points, yielding values of 0.993, 0.886, and 0.931, respectively. Moreover, the prediction determination coefficients (R_p^2) were also computed and found to be 0.986, 0.834, and 0.928 for the respective time intervals. According to the R_c^2 and R_p^2 in the model results of PLS of Pb^{2+}, Ni^{2+}, and Co^{2+} experiment in Sections 3.1.2, 3.2.2, and 3.3.2 the best times are 10 min, 20 min, and 30 min. Therefore, we believe that 10 min, 20 min, and 30 min are the judgment times of Pb^{2+}, Ni^{2+}, and Co^{2+}.

3.5. *Study on concentration of Pb^{2+}, Ni^{2+} and Co^{2+} in real soil based on PLS*

To evaluate the predictive accuracy and robustness of the integrated solution model introduced in Section 3.4, a comprehensive analysis was conducted on a set of representative surface soil samples. These samples were collected from locations surrounding five distinct heavy industry bases within the Yangtze River Delta region, namely the Shanghai chemical plant, Hangzhou Xiaoshan No.4 Chemical Plant, Ningbo Beilun District Jiangnan Electroplating Factory, Huainan cement plant, and Nanjing electroplating factory. Number five soil samples in sequence, numbered 1–5. After removing surface debris, collect topsoil and test the

Table 5
PLS model parameters under mixed solution stress.

Discrimination model	Calibration		Prediction	
	R_c^2	RMSC	R_p^2	RMSEP
10 min	0.993	0.148	0.986	0.223
20 min	0.886	0.296	0.834	0.416
30 min	0.931	0.205	0.928	0.289

characteristics of the soil according to the testing standards. The results are shown in Table 6. Due to the larger particle size of soil No.2, we adopted another testing method, and the test results are shown in Table 7.

Dry the collected soil samples uniformly at low temperatures, and sieve, or crush them to ensure a uniform soil particle size. Add distilled water and mix it with soil samples to form a soil suspension. Add the soil suspension to the oscillator for oscillation, mix it evenly, and let it stand for some time until full contact between the soil suspension and water. Next, filter the soil suspension using a membrane filter to obtain a water-soluble solution of heavy metals. Pour the filtered solution into a beaker and evaporate the moisture using a hot plate. Add the concentrated solution to a test tube, dilute it with distilled water until the liquid volume is consistent, and obtain a water-soluble heavy metal solution of the soil. At the same time, we used the traditional method of AAS to detect the content of water-soluble heavy metals Pb^{2+}, Ni^{2+}, and Co^{2+} in these 5 soil samples. According to the dissolution rate formula in Section 2.3, the water-soluble heavy metals Pb^{2+}, Ni^{2+}, and Co^{2+} in the five soil samples are shown in Table 8. The concentration types of soil samples in Table 8 correspond to samples 1, 5, and 9 in Table 4 of Section 3.4. Therefore, we used the AAS method as an accuracy reference for the water-soluble heavy metal content in the soil sample. We used the correlation model between terahertz spectral absorbance changes and heavy metal ion concentrations established in Table 4 to predict the content of Pb^{2+}, Ni^{2+}, and Co^{2+} in the soil sample, and calculate the prediction accuracy.

Introduce *S. obliquus* into water-soluble heavy metal solutions prepared from five soil samples. Collect 6 samples from each solution at 10, 20, and 30 minutes, for a total of 30 samples, and collect terahertz spectra at 3.5–5 THz and 8–10 THz. Utilizing PLS models to predict the spectral data gathered from all 30 samples. The correlation model between terahertz spectral absorbance changes and heavy metal ion concentrations established in Section 3.4, Table 4, was used to determine the prediction accuracy of real soil samples, as shown in Table 9. In this experiment, the average prediction accuracy of Pb^{2+} was 97.8 %, the average prediction accuracy of Ni^{2+} was 91.8 %, and the average prediction accuracy of Co^{2+} was 90 %. This result also indicates that the more toxic Pb^{2+} has a greater impact on *S. obliquus* and is more easily detected in a short period than Ni^{2+} and Co^{2+}.

4. Discussion and prospects

The research focuses on analyzing the terahertz spectra of *S. obliquus* exposed to toxic heavy metals (Pb^{2+}, Ni^{2+}, Co^{2+}) at different time intervals (10, 20, 30 min). Effects of stress on *S. obliquus* of varying purities were explored, with spectroscopic data used to determine the responses to different metal stress conditions. Using PLS analysis, optimal detection times were established: 10 min for Pb^{2+}, 20 min for Ni^{2+}, and 30 min for Co^{2+}. Pb^{2+} exhibited higher toxicity than Ni^{2+} and Co^{2+}. Then, based on the reference of water-soluble heavy metal content detected by the AAS method in soil, a correlation model between terahertz spectral absorbance changes and heavy metal ion concentration was established using PLS, and the content of Pb^{2+}, Ni^{2+}, and Co^{2+} in soil samples was predicted. The results showed that the accuracy rates were 97.8 % for Pb^{2+}, 91.8 % for Ni^{2+}, and 90 % for Co^{2+}. The proposed PLS model eliminates the complex pretreatment of soil samples. The pretreatment time was reduced from over 20 hours to 0.5 hours. The sample volume decreased from 50 ml to 5 ml, enhancing the accuracy from 1 μg/L to 0.1 μg/L. This methodology advances environmental monitoring by efficiently detecting heavy metal stress in soil, enhancing soil health assessment, and promoting ecological sustainability.

Under normal circumstances, the content of heavy metals in soil is correlated with soil characteristics such as particle size, water content, and organic matter content. However, in this study, we collected five samples with significant differences in soil characteristics. After processing and testing, we found that there was no specific pattern in the results of the five soil characteristic differences (average particle size, pH, organic matter content, water content, and catch exchange capacity) and heavy metal content, which may be related to the large regional differences in soil sample collection. Meanwhile, after unified sample processing, soil characteristics had no significant impact on the prediction accuracy of PLS models, and the detection accuracy was above 90 %. This research method successfully detected the content of water-soluble heavy metals that undergo physical migration and transformation in soil solutions.

Table 7
The average particle size of soil No.2*.

Average particle size (mm)	Proportion (%)	Testing standard
+5	24.58	GB/T 21524–2008
5–2	9.47	
2–1	10.01	
1–0.5	11	
0.5–0.25	10.71	
0.25–0.01	10.20	
0.01–0.075	4.37	
−0.075	19.66	

Table 8
Measurement of water-soluble heavy metal content in soil by AAS.

Samples	Test results (μg/L)		Sample types
1	Pb^{2+} , Ni^{2+} , Co^{2+}	<20 , 20 , \	Approximately Sample 1
2			
3		\ , 20 , 50	Sample 5
4			
5		<20 , \ , 50	Approximately Sample 9

Table 9
Prediction accuracy of real soil samples.

Accuracy	Pb^{2+}(10 min)	Ni^{2+}(20 min)	Co^{2+} (30 min)
1	93 %	100 %	93 %
2	100 %	93 %	85 %
3	100 %	83 %	100 %
4	100 %	90 %	86 %
5	93 %	93 %	86 %
Summary	97.8 %	91.8 %	90 %

Table 6
Soil samples characteristics.

Samples	Average particle size (μm)	D50 (μm)	D97 (μm)	pH	Organic matter content (g/kg)	Water content (%)	Cation exchange capacity (cmol+/kg)
1	57.502	24.235	391.244	7.27	24.1	36.3	16.2
2	*	*	*	8.11	16.3	6.2	13.2
3	59.013	22.185	465.357	8.43	15	18	12.5
4	85.208	28.115	536.443	7.98	20.4	27.9	14.7
5	90.417	25.926	544.592	8.76	16.4	47.3	10.8
Testing standard	GB/T 19077–2016			HJ 962–2018	NY/T 1121.6–2006	LY/T 1215–1999	HJ 889–2017

The migration forms of heavy metals in soil are diverse, and the soil presents a complex structural composition, including not only solid-phase substances but also liquid and gas-phase substances [43]. Heavy metal ions undergo various migration and transformation processes in soil, mainly involving physical, chemical, and biological transformations [44]. In the future, we will collect more soil samples and conduct in-depth research on the interaction mechanism between soil characteristics and heavy metal ions by controlling variables and using terahertz spectroscopy technology. In addition, the rapid detection of other types of heavy metal content is expected to have great research prospects in the field of soil testing.

CRediT authorship contribution statement

Yuxin Zhou: Writing – review & editing, Writing – original draft, Investigation, Formal analysis, Data curation. **Di Zhu:** Writing – original draft, Methodology, Data curation. **Yan Peng:** Supervision, Resources, Project administration, Funding acquisition, Conceptualization. **Yiming Zhu:** Supervision, Resources, Project administration, Funding acquisition, Conceptualization. **Yongni Shao:** Writing – review & editing, Supervision, Resources, Project administration, Funding acquisition, Conceptualization.

Declaration of Competing Interest

The authors declare that they have no known competing financial interests or personal relationships that could have appeared to influence the work reported in this paper.

Data availability

Data will be made available on request.

Acknowledgements

The research presented in this article was supported by the National Major Project (grant numbers 2017YFA0701005), Natural Fund Project of Shanghai (grant numbers 21ZR1444700), National Natural Science Foundation of China (grant numbers 61988102).

References

[1] O.I. Davutluoglu, G. Seckin, C.B. Ersu, et al., Heavy metal content and distribution in surface sediments of the Seyhan River, Turkey, J. Environ. Manag. 92 (2011) 2250–2259, https://doi.org/10.1016/j.jenvman.2011.04.013.
[2] N. Gaur, G. Flora, M. Yadav, et al., A review with recent advancements on bioremediation-based abolition of heavy metals, Environ. Sci.: Process. Impacts 16 (2014) 180–193, https://doi.org/10.1039/C3EM00491K.
[3] K.P. Mishra, Lead exposure and its impact on immune system: a review, Toxicol. Vitr. 23 (2009) 969–972, https://doi.org/10.1016/j.tiv.2009.06.014.
[4] K.S. Cameron, V. Buchner, P.B. Tchounwou, Exploring the molecular mechanisms of nickel-induced genotoxicity and carcinogenicity: a literature review 26 (2011) 81–92, https://doi.org/10.1515/reveh.2011.012.
[5] A.T. Ubando, A.D.M. Africa, M.C. Maniquiz-Redillas, et al., Microalgal biosorption of heavy metals: a comprehensive bibliometric review, J. Hazard. Mater. 402 (2021) 123431, https://doi.org/10.1016/j.jhazmat.2020.123431.
[6] R.-Y. Kim, J.-K. Yoon, T.-S. Kim, et al., Bioavailability of heavy metals in soils: definitions and practical implementation—a critical review, Environ. Geochem. Health 37 (2015) 1041–1061, https://doi.org/10.1007/s10653-015-9695-y.
[7] R. Sun, Y. Gao, Y. Yang, Leaching of heavy metals from lead-zinc mine tailings and the subsequent migration and transformation characteristics in paddy soil, Chemosphere 291 (2022) 132792, https://doi.org/10.1016/j.chemosphere.2021.132792.
[8] M. Taghipour, M. Jalali, Effects of some industrial and organic wastes application on growth and heavy metal uptake by tomato (Lycopersicum esculentum) grown in a greenhouse condition, Environ. Sci. Pollut. Res. 27 (2020) 5353–5366, https://doi.org/10.1007/s11356-019-07017-6.
[9] C. Moor, T. Lymberopoulou, V.J. Dietrich, Determination of heavy metals in soils, sediments and geological materials by ICP-AES and ICP-MS, Microchim. Acta 136 (2001) 123–128, https://doi.org/10.1007/s006040170041.
[10] T. Stafilov, R. Šajn, L. Ahmeti, Geochemical characteristics of soil of the city of Skopje, Republic of Macedonia, J. Environ. Sci. Health, Part A 54 (2019) 972–987, https://doi.org/10.1080/10934529.2019.1620042.
[11] J.Q. McComb, C. Rogers, F.X. Han, et al., Rapid screening of heavy metals and trace elements in environmental samples using portable X-ray fluorescence spectrometer, a comparative study, Water Air Soil Pollut. 225 (2014) 2169, https://doi.org/10.1007/s11270-014-2169-5.
[12] R. Ravansari, S.C. Wilson, M. Tighe, Portable X-ray fluorescence for environmental assessment of soils: not just a point and shoot method, Environ. Int. 134 (2020) 105250, https://doi.org/10.1016/j.envint.2019.105250.
[13] P. Kurup, C. Sullivan, R. Hannagan, et al., A review of technologies for characterization of heavy metal contaminants, Indian Geotech. J. 47 (2017) 421–436, https://doi.org/10.1007/s40098-016-0214-6.
[14] S.B. Ummalyma, R.K. Sukumaran, Cultivation of microalgae in dairy effluent for oil production and removal of organic pollution load, Bioresour. Technol. 165 (2014) 295–301, https://doi.org/10.1016/j.biortech.2014.03.028.
[15] J. Umamaheswari, R. Rajamanickam, S. Vilvanathan et al., *Removal of Heavy Metals and Organic Pollutants by Marine Microalgae, in Marine Organisms: A Solution to Environmental Pollution? Uses in Bioremediation and in Biorefinery*, T. Encarnação, A. Canelas Pais Eds., Springer International Publishing, Cham, 2023, pp. 29-64 978-3-031-17226-7 https://doi.org/10.1007/978-3-031-17226-7_3.
[16] I. Anastopoulos, G.Z. Kyzas, Progress in batch biosorption of heavy metals onto algae, in: Journal of Molecular Liquids, **209**, 2015, pp. 77–86, https://doi.org/10.1016/j.molliq.2015.05.023.
[17] Y.K. Leong, J.-S. Chang, Bioremediation of heavy metals using microalgae: recent advances and mechanisms, Bioresour. Technol. 303 (2020) 122886, https://doi.org/10.1016/j.biortech.2020.122886.
[18] M. Danouche, N. El Ghachtouli, H. El Arroussi, Phycoremediation mechanisms of heavy metals using living green microalgae: physicochemical and molecular approaches for enhancing selectivity and removal capacity, Heliyon 7 (2021) e07609, https://doi.org/10.1016/j.heliyon.2021.e07609.
[19] O. Spain, M. Plöhn, C. Funk, The cell wall of green microalgae and its role in heavy metal removal, Physiol. Plant. 173 (2021) 526–535, https://doi.org/10.1111/ppl.13405.
[20] Y.N. Shao, Y.T. Wang, D. Zhu, et al., Measuring heavy metal ions in water using nature existed microalgae as medium based on terahertz technology, J. Hazard. Mater. 435 (2022), https://doi.org/10.1016/j.jhazmat.2022.129028.
[21] H. Quiquampoix, R.G. Burns, Interactions between proteins and soil mineral surfaces: environmental and health consequences, Elements 3 (2007) 401–406, https://doi.org/10.2113/GSELEMENTS.3.6.401.
[22] M.R. Islam, B. Singh, F.A. Dijkstra, Stabilisation of soil organic matter: interactions between clay and microbes, Biogeochemistry 160 (2022) 145–158, https://doi.org/10.1007/s10533-022-00956-2.
[23] K. Greeshma, H.-S. Kim, R. Ramanan, The emerging potential of natural and synthetic algae-based microbiomes for heavy metal removal and recovery from wastewaters, Environ. Res. 215 (2022) 114238, https://doi.org/10.1016/j.envres.2022.114238.
[24] J. Cheng, W. Yin, Z. Chang, et al., Biosorption capacity and kinetics of cadmium(II) on live and dead Chlorella vulgaris, J. Appl. Phycol. 29 (2017) 211–221, https://doi.org/10.1007/s10811-016-0916-2.
[25] S. Sakamoto, K. Yoshida, S. Sugihara, et al., Development of a new high-throughput method to determine the composition of ten monosaccharides including 4-O-methyl glucuronic acid from plant cell walls using ultra-performance liquid chromatography, Plant Biotechnol. 32 (2015) 55–63, https://doi.org/10.5511/plantbiotechnology.15.0113a.
[26] C. Pasquini, Near infrared spectroscopy: a mature analytical technique with new perspectives – a review, Anal. Chim. Acta 1026 (2018) 8–36, https://doi.org/10.1016/j.aca.2018.04.004.
[27] H.J. Butler, L. Ashton, B. Bird, et al., Using Raman spectroscopy to characterize biological materials, Nat. PROTOCOLS 11 (2016) 664–687, https://doi.org/10.1038/nprot.2016.036.
[28] T. Hong, J.-Y. Yin, S.-P. Nie, et al., Applications of infrared spectroscopy in polysaccharide structural analysis: progress, challenge and perspective, Food Chem.: X 12 (2021) 100168, https://doi.org/10.1016/j.fochx.2021.100168.
[29] Z. Li, J. Wang, D. Li, Applications of Raman spectroscopy in detection of water quality, Appl. Spectrosc. Rev. 51 (2016) 333–357, https://doi.org/10.1080/05704928.2015.1131711.
[30] Y. Guo, W. Jin, W. Wang, et al., Baseline correction for Raman spectra using a spectral estimation-based asymmetrically reweighted penalized least squares method, Appl. Opt. 62 (2023) 4766–4776, https://doi.org/10.1364/AO.489478.
[31] S.J. Barton, B.M. Hennelly, An algorithm for the removal of cosmic ray artifacts in spectral data sets, Appl. Spectrosc. 73 (2019) 893–901, https://doi.org/10.1177/0003702819839098.
[32] M. Gezimati, G. Singh, Terahertz imaging and sensing for healthcare: current status and future perspectives, IEEE Access 11 (2023) 18590–18619, https://doi.org/10.1109/ACCESS.2023.3247196.
[33] Y. Peng, J. Huang, J. Luo, et al., Three-step one-way model in terahertz biomedical detection, PhotoniX 2 (2021) 12, https://doi.org/10.1186/s43074-021-00034-0.
[34] Y. Wang, J. Xue, Q. Wang, et al., Structural investigation of a 2:1 co-crystal between diflunisal and isonicotinamide based on terahertz and Raman spectroscopy, Spectrochim. Acta Part A: Mol. Biomol. Spectrosc. 216 (2019) 98–104, https://doi.org/10.1016/j.saa.2019.03.023.
[35] M. Takahashi, N. Okamura, X. Ding, et al., Intermolecular hydrogen bond stretching vibrations observed in terahertz spectra of crystalline vitamins, CrystEngComm 20 (2018), https://doi.org/10.1039/C8CE00095F.
[36] H. Wang, F. Zheng, Y. Xu, et al., Recent progress in terahertz biosensors based on artificial electromagnetic subwavelength structure, TrAC Trends Anal. Chem. 158 (2023) 116888, https://doi.org/10.1016/j.trac.2022.116888.

[37] Y. Wang, Q. Wang, Z. Zhao, et al., Rapid qualitative and quantitative analysis of chlortetracycline hydrochloride and tetracycline hydrochloride in environmental samples based on terahertz frequency-domain spectroscopy, Talanta 190 (2018) 284–291, https://doi.org/10.1016/j.talanta.2018.08.008.
[38] C.F. Carolin, P.S. Kumar, A. Saravanan, et al., Efficient techniques for the removal of toxic heavy metals from aquatic environment: a review, J. Environ. Chem. Eng. 5 (2017) 2782–2799, https://doi.org/10.1016/j.jece.2017.05.029.
[39] C.U. Stehle, W. Abuillan, B. Gompf, et al., Far-infrared spectroscopy on free-standing protein films under defined temperature and hydration control, J. Chem. Phys. 136 (2012) 075102, https://doi.org/10.1063/1.3686886.
[40] F.L. Jiang, I. Ikeda, Y. Ogawa, et al., Terahertz absorption spectra of fatty acids and their analogues, J. Oleo Sci. 60 (2011) 339–343, https://doi.org/10.5650/jos.60.339.
[41] F.L. Jiang, I. Ikeda, Y. Ogawa, et al., Rapid determination of saponification value and polymer content of vegetable and fish oils by terahertz spectroscopy, J. Oleo Sci. 61 (2012) 531–535, https://doi.org/10.5650/jos.61.531.
[42] S. Nakajima, K. Shiraga, T. Suzuki, et al., Quantification of starch content in germinating mung bean seedlings by terahertz spectroscopy, Food Chem. 294 (2019) 203–208, https://doi.org/10.1016/j.foodchem.2019.05.065.
[43] C. Qu, W. Chen, X. Hu, et al., Heavy metal behaviour at mineral-organo interfaces: Mechanisms, modelling and influence factors, Environ. Int. 131 (2019) 104995, https://doi.org/10.1016/j.envint.2019.104995.
[44] W. Su, X. Li, H. Zhang, et al., Migration and transformation of heavy metals in hyperaccumulators during the thermal treatment: a review, Environ. Sci. Pollut. Res. 28 (2021) 47838–47855, https://doi.org/10.1007/s11356-021-15346-8.